

# High-throughput scanning confocal microscope for single molecule analysis

Chandran R. Sabanayagam, John S. Eid, and Amit Meller<sup>a)</sup>

Rowland Institute at Harvard, Harvard University, 100 Edwin H. Land Boulevard, Cambridge, Massachusetts 02142

(Received 29 October 2003; accepted 17 December 2003)

An automated and programmable confocal microscope that can acquire upwards of  $10^3$  single-molecule fluorescence resonance energy transfer (FRET) time traces is presented. The microscope augments the capabilities of current instruments by employing a flow cell that allows full control of the sample's chemical environment, automatic locating and probing of single molecules, and an automatic focusing feature that enables the unattended scanning of large areas of the sample. This microscope performs routine acquisition of thousands of single-molecule events, in a highly reproducible fashion. These capabilities were utilized in recording the distributions of FRET efficiencies arising from control DNA molecules specifically labeled with internal donor-acceptor reporters. © 2004 American Institute of Physics. [DOI: 10.1063/1.1646725]

Recent progress in optical imaging of single molecules (SM) has made it possible to study the structure and interactions of individual biomolecules using single-pair fluorescence resonance energy transfer (FRET) reporters.<sup>1,2</sup> Some recent examples of SM detection to study molecular interactions include: DNA structural rearrangements,<sup>3,4</sup> ribozyme kinetics,<sup>5</sup> protein and peptide conformational dynamics,<sup>6,7</sup> and enzyme kinetics.<sup>8</sup> The hallmark of the SM technique is that the probed signals are not masked by the averaging nature of ensemble measurements. Thus, rare and fast fluctuations and inhomogeneities among putatively identical molecules can be observed, enabling the differentiation between normal distributions and skewed ones resulting from non-Markovian and/or nonergodic processes.<sup>9</sup> However, thousands of SM traces are required to allow the adequate sampling of the phase space.

Large area detectors such as cooled CCD cameras have the capacity of probing  $\sim 100$  SM traces simultaneously, but are limited in their temporal resolution to  $\sim 100$  ms.<sup>5</sup> Point detectors, such as avalanche photodiodes, have submicrosecond resolution, allowing one to probe fast fluctuations in FRET<sup>7</sup> and variations in fluorescence lifetime.<sup>10</sup> In order to circumvent the labor-intensive tasks of manually probing thousands of individual molecules, we have developed a robust and high throughput method that allows one to acquire  $\sim 10^3$  SM traces overnight in an unattended manner. The main features in our instrument that made this task possible are: (1) automatic focusing, (2) automatic locating and tracing of individual molecules, and (3) a temperature regulated flow cell. Our custom designed flow cell allows for continuous buffer exchange, which is necessary to maintain constant chemical conditions in the sample for long periods of time. In addition, our flow cell permits easy exchange of buffers.

To test the instrument we prepared a model 30 basepair DNA hairpin molecule internally labeled with donor-acceptor pairs. The DNA sequence is:

5'-CCGTCCTGATTTATTTCTGGGTTCTGTTGCTT[b]TTGCAACAGAACCCAGAAA[r]AAA[5]CAGGACGG-3', where [b] denotes biotin-dT (for immobilization onto streptavidin surfaces), [r] denotes tetramethylrhodamine-dT (donor), and [5] Cy5-dT (acceptor), connected via 6-carbon linkers. The fluorophores were separated by four basepairs on the same strand of the duplex. The separation between the fluorophores (4–5 nm) is comparable to the 5.3 nm Förster radius of the FRET pair,<sup>11</sup> yielding relatively high and steady FRET efficiencies.

Our optical design is schematically described in Fig. 1.<sup>12</sup> The 514.5 nm line of an Ar<sup>+</sup> laser (Spectra-Physics)

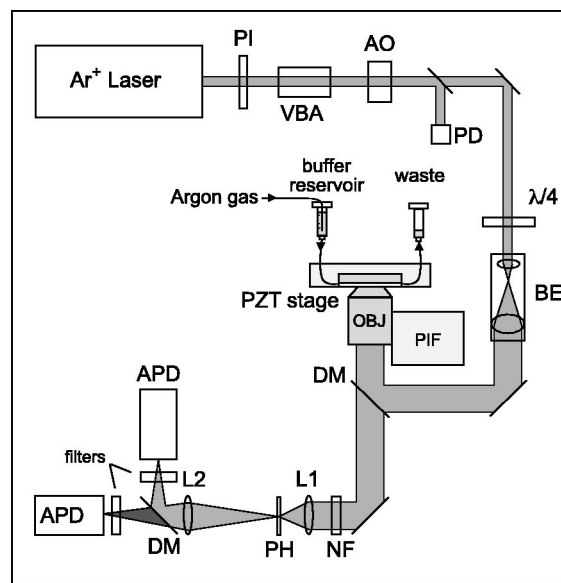


FIG. 1. Schematic illustration of the optical setup. The excitation source was the 514.5 nm line from an Ar<sup>+</sup> laser, coupled via a single mode optical fiber. The various components are: linear polarizer (P1), variable beam attenuator (VBA), acousto-optical modulator (AO), photodiode (PD), quarter waveplate ( $\lambda/4$ ), 3 $\times$  beam expander (BE), dichroic mirror (DM), piezo focusing translator (PIF), objective (OBJ), 514.5 nm notch filter (NF), 75 mm lens (L1), 50  $\mu$ m pinhole (PH), 150 mm lens (L2), and avalanche photodiode (APD).

<sup>a)</sup>Author to whom correspondence should be addressed; electronic mail: meller@rowland.harvard.edu

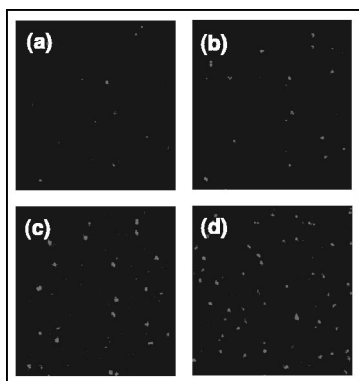


FIG. 2. Real time imaging of the surfaces ( $20 \times 20 \mu\text{m}^2$ , acceptor channel) during the binding process provides control over the surface coverage density. (a) to (d) represent a time series of the same area 2, 5, 10 and 15 min after initial exposure of the surface to 2.5 pM of biotinylated, FRET-labeled hairpin.

was cleaned, attenuated, and circularly polarized (with a zero order quarter waveplate). The expanded beam was directed vertically using a dichroic mirror (Chroma) into the back aperture of a  $63\times$ , 1.4 NA, oil immersion objective (Zeiss) mounted on a nanopositioner (Physik Instrumente). The emitted light was filtered by a notch filter (Kaiser optics) and a  $50 \mu\text{m}$  pinhole. The pinhole image was spectrally split using a 640 nm dichroic mirror (Chroma), and projected with 1:1 magnification onto two APDs (Perkin Elmer AQR14). Cross-talk was removed using the appropriate filters, resulting in 15% leakage of the donor emission into the acceptor channel, and a negligible level of acceptor to donor leakage.

Our flow cell was made by fusing a patterned, 1-mm-thick, polydimethylsilicone (PDMS) disk to a freshly cleaned quartz coverslip. The PDMS disk consisted of three  $30 \mu\text{l}$  rectangular chambers that were accessed by inlet and outlet syringe needles connected to a buffer reservoir and a pump, respectively. The flow cell was supported on its back side by a sapphire window, and placed in a custom made cell holder containing a water cooled thermoelectric element (allowing temperature regulation to within  $0.05^\circ\text{C}$ ).

An algorithm for the automated location of immobilized SMs using point detectors has been described by Ha *et al.*<sup>13</sup> Here we present an alternative approach, which permits the unattended scanning of large areas ( $\sim\text{cm}^2$ ) in the sample. The sample cell was mounted on a motorized  $xy$  stage allowing coarse (up to 25 mm), and fine ( $\sim 1 \text{ nm}$ ) motion using two PZT actuators (Physik Instrumente). A custom control and data acquisition program written in LABVIEW (National Instruments) was first used to scan  $20 \times 20 \mu\text{m}^2$  areas at  $0.2 \mu\text{m}$  resolution, with a rate of  $0.1 \mu\text{m}/\text{ms}$ . The positions of the PZT actuators were directly read during the scan using an A/D board sharing the same clock with a counter board (both National Instruments) used to acquire the photon counts. The data were immediately processed to yield the intensity-weighted locations of all pixels above the background counts. A typical surface density was 50 clusters per scan [Fig. 2(d)]. The stage was then programmed to move to a new origin  $100 \mu\text{m}$  away, and the scanning process was repeated. The auto-focusing mode consists of eight scans at successive  $z$  positions in  $0.2 \mu\text{m}$  steps. The best  $z$  value was

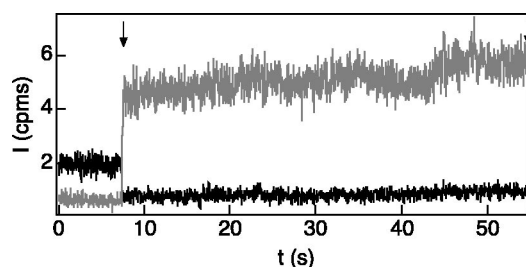


FIG. 3. Time trace of single-pair FRET on a DNA hairpin. A characteristic trace showing acceptor (black) photobleaching concurrent with an increase in donor fluorescence (gray) at  $t=8 \text{ s}$ . At  $t=55 \text{ s}$  the donor photobleaches and the donor and acceptor intensities drop to the background level. The transitions are indicated by arrows. The 50 kHz raw data were binned to 10 ms for display purposes.

determined by the scan that produced the maximum number of clusters.

The cells were activated with streptavidin following the procedures employed by others.<sup>3,5,14</sup> Approximately 2.5 pM of biotinylated, labeled DNA hairpin was then injected into the cell. Binding of the fluorescent, biotinylated, molecules to the surface was monitored in real time to achieve the desired coverage [Figs. 2(a)–2(d)]. The glucose oxidase/catalase enzymatic  $\text{O}_2$  scavenging system was used to decrease the photobleaching rate of the fluorophores during SM tracing.<sup>15</sup>

Figure 3 displays an example of a typical SM trace in which the acceptor photobleaches before the donor. To increase the acquisition throughput, we implemented a real time feedback control that stops data acquisition 0.5 s after both the donor and acceptor intensities fall below a photobleaching threshold (1 cpms, twice the background level). The laser intensity ( $1.7 \text{ kW}/\text{cm}^2$  at the sample) was set below the fluorophores' saturation level (data not shown). Raw fluorescence time trace data collected at 50 kHz were binned to 1 ms for signal analysis, and the FRET efficiency was calculated as previously described.<sup>16</sup> The FRET data were analyzed by convoluting the median-filtered data with a mask kernel,<sup>17</sup> to identify segments (down to 10 ms) separated by sharp transitions. The average FRET value of each segment was used to construct the efficiency histogram.

Figure 4(a) represents the result of a typical data set (1435 molecules). Two FRET levels are apparent in the distribution: A lower level peak ( $E \approx 0.01$ ) representing donor only contributions (the small deviation from zero is primarily due to errors in the estimation of  $\beta^{16}$ ), and a high FRET peak ( $E \approx 0.75$ ). In Fig. 4(b) we display the distribution of segment lengths of both low and high FRET levels. These distributions are well described by single exponentials with  $1/e$  values of 7.7 and 3.5 s, which represent the average photobleaching time of the donor and acceptor, respectively. The appearance of a single exponential decay time indicates that the control DNA molecules do not exhibit fast fluctuations (bound by the 10 ms resolution of our segment analysis), as expected. In fact, over 90% of the molecules are represented by only two segments, as in Fig. 3. Thus in Fig. 4(a) each molecule is equally weighted, and the variations between molecules is the prominent contributor to the width of the FRET distribution. In the more traditional treatment, SM FRET histograms are constructed from time bins<sup>18</sup> (e.g., 25

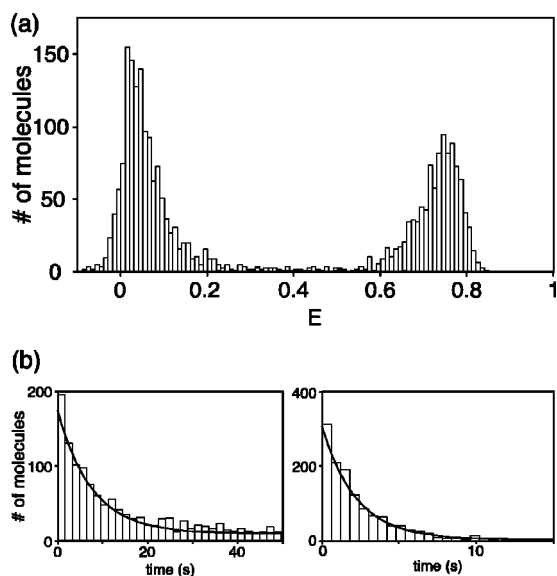


FIG. 4. (a) Distribution of FRET efficiencies from DNA hairpins. To construct the histogram, FRET time traces were automatically acquired overnight from 1435 molecules. The efficiencies were calculated by averaging the low and high FRET segments of each molecule. (b) Duration distributions of the low (left panel) and high (right panel) FRET levels, approximated by single exponential functions. The  $1/e$  values are 7.7 and 3.5 s for the low and high levels, respectively.

ms) of all acquired traces. We note that this analysis is biased toward the long-lived molecules.

To summarize, the implementation of a high throughput confocal microscope was demonstrated by testing a control DNA hairpin that exhibits two FRET levels. Using point detectors allows one to collect photons with high temporal resolution, i.e., 50 kHz or more, which provides additional insight to FRET variations.<sup>19</sup> The segment analysis applied to our data preserves the history of FRET fluctuations in each trace, but required binning of the data to 10 ms (photon limited). Other forms of analysis (e.g., autocorrelation) can be directly applied to the 50 kHz data with a concurrent loss of the time trajectory information. The automatic focusing feature of the instrument is extremely robust, thus allowing experiments to continue over long periods of time under well-defined conditions. The use of real time analysis to identify photobleaching events enhances the throughput of the instrument, by enabling the observation of rare, long-lived fluorescent molecules in a time-efficient manner.

The authors thank Dr. M. Burns, D. Koster, and the Rowland Institute at Harvard (staff and financial support).

- <sup>1</sup> S. Weiss, *Science* **283**, 1676 (1999); *Nat. Struct. Biol.* **7**, 724 (2000); T. Ha, Th. Enderle, D. F. Ogletree, D. S. Chemla, P. R. Selvin, and S. Weiss, *Proc. Natl. Acad. Sci. U.S.A.* **93**, 6264 (1996); S. Nie and R. N. Zare, *Annu. Rev. Biophys. Struct.* **26**, 567 (1997).
- <sup>2</sup> P. W. Ambrose, P. M. Goodwin, J. H. Jett, A. Van Orden, J. H. Werner, and R. A. Keller, *Chem. Rev. (Washington, D.C.)* **99**, 2929 (1999).
- <sup>3</sup> J. R. Grunwell, J. L. Glass, T. D. Lacoste, A. A. Deniz, D. S. Chemla, and P. Schultz, *J. Am. Chem. Soc.* **123**, 4295 (2001).
- <sup>4</sup> S. A. McKinney, A.-C. Déclais, D. M. J. Lilley, and T. Ha, *Nat. Struct. Biol.* **10**, 93 (2003).
- <sup>5</sup> For example, see X. Zhuang, L. B. Bartley, H. P. Babcock, R. Russell, T. Ha, D. Herschlag, and S. Chu, *Science* **288**, 2048 (2000).
- <sup>6</sup> T. Ha, A. Y. Ting, J. Liang, W. B. Caldwell, A. A. Deniz, D. S. Chemla, P. G. Schultz, and S. Weiss, *Proc. Natl. Acad. Sci. U.S.A.* **96**, 893 (1999); E. Rhoades, E. Gussakovskiy, and G. Haran, *ibid.* **100**, 3197 (2003).
- <sup>7</sup> D. S. Talaga, W. L. Lau, H. Roder, J. Tang, Y. Jia, W. F. DeGrado, and R. M. Hochstrasser, *Proc. Natl. Acad. Sci. U.S.A.* **97**, 13021 (2000).
- <sup>8</sup> H. P. Lu, L. Xun, and S. X. Xie, *Science* **282**, 1877 (1998); S. X. Xie and H. P. Lu, *J. Biol. Chem.* **274**, 15967 (1999).
- <sup>9</sup> X. Brokmann, J.-P. Hermier, G. Messin, P. Desbiolles, J.-P. Bouchaud, and M. Dahan, *Phys. Rev. Lett.* **90**, 120601 (2003).
- <sup>10</sup> M. Lee, J. Tang, and R. M. Hochstrasser, *Chem. Phys. Lett.* **344**, 501 (2001); P. Tinnefeld, D.-P. Herten, and M. Sauer, *J. Phys. Chem. A* **105**, 7989 (2001); D. Hu and P. Lu, *J. Phys. Chem. B* **107**, 618 (2003).
- <sup>11</sup> A. A. Deniz, M. Dahan, J. R. Grunwell, T. Ha, A. E. Faulhaber, D. S. Chemla, S. Weiss, and P. G. Schultz, *Proc. Natl. Acad. Sci. U.S.A.* **96**, 3670 (1999).
- <sup>12</sup> G. Bonnet, O. Krichevsky, and A. Libchaber, *Proc. Natl. Acad. Sci. U.S.A.* **95**, 8602 (1998).
- <sup>13</sup> T. Ha, D. S. Chemla, Th. Enderle, and S. Weiss, *Appl. Phys. Lett.* **70**, 782 (1997).
- <sup>14</sup> V. T. Moy, E. L. Florin, and H. E. Gaub, *Science* **266**, 257 (1994).
- <sup>15</sup> Y. Harada, K. Sakurada, T. Aoki, D. D. Thomas, and T. Yanagida, *J. Mol. Biol.* **216**, 49 (1990).
- <sup>16</sup> FRET efficiency was calculated similarly to previously discussed (Ref. 18). We used  $E = (I_A - \beta I_D) / (I_A + \gamma I_D)$ , where  $I_A$  and  $I_D$  are the intensities of the acceptor and donor channels, respectively. The factor  $\beta$  represents the leakage of the donor into the acceptor channel, and  $\gamma$  is the ratio of the probing efficiencies in the two channels multiplied by the fluorophores' quantum yield ratio. In practice, the correction factors were determined according to:  $\beta = I'_A / I'_D$  and  $\gamma = \Delta I'_A / \Delta I'_D$ , where  $I'_A$  and  $I'_D$  are the channels' intensities after the acceptor photobleaches in each event, and  $\Delta I'$  represents the change in each channel intensity before and after the acceptor photobleaches. Mean and standard deviation values for  $\beta$  and  $\gamma$  were  $0.15 \pm 0.05$  and  $0.7 \pm 0.25$ , respectively.
- <sup>17</sup> G. Haran, *J. Phys.: Condens. Matter* **15**, R1291 (2003).
- <sup>18</sup> T. Ha, A. Y. Ting, J. Liang, A. A. Deniz, D. S. Chemla, P. G. Schultz, and S. Weiss, *Chem. Phys.* **247**, 107 (1999); Y. Jia, D. S. Talaga, W. L. Lau, H. S. M. Lu, W. F. DeGrado, and R. M. Hochstrasser, *ibid.* **247**, 69 (1999).
- <sup>19</sup> G. F. Schröder and H. Grubmüller, *J. Chem. Phys.* **119**, 9920 (2003).